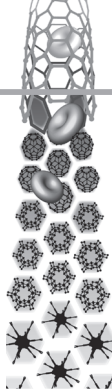


For reprint orders, please contact: [reprints@futuremedicine.com](mailto:reprints@futuremedicine.com)

# Vascular-targeted photothermal therapy of an orthotopic murine glioma model



**Aim:** To develop nanoshells for vascular-targeted photothermal therapy of glioma. **Materials & methods:** The ability of nanoshells conjugated to VEGF and/or poly(ethylene glycol) (PEG) to thermally ablate VEGF receptor-2 positive endothelial cells upon near-infrared laser irradiation was evaluated *in vitro*. Subsequent *in vivo* studies evaluated therapy in mice bearing intracerebral glioma tumors by exposing tumors to near-infrared light after systemically delivering saline, PEG-coated nanoshells, or VEGF-coated nanoshells. The treatment effect was monitored with intravital microscopy and histology. **Results:** VEGF-coated but not PEG-coated nanoshells bound VEGF receptor-2 positive cells *in vitro* to enable targeted photothermal ablation. *In vivo*, VEGF targeting doubled the proportion of nanoshells bound to tumor vessels and vasculature was disrupted following laser exposure. Vessels were not disrupted in mice that received saline. The normal brain was unharmed in all treatment and control mice. **Conclusion:** Nanoshell therapy can induce vascular disruption in glioma.

Original submitted 27th September 2011; Revised submitted 12th December 2011

**KEYWORDS:** antiangiogenic therapy ■ brain tumor ■ cancer ■ glioma ■ nanoparticles ■ near-infrared ■ thermal therapy ■ VEGF

Emily S Day<sup>1</sup>, Linna Zhang<sup>2</sup>, Patrick A Thompson<sup>2</sup>, Janice A Zawaski<sup>2</sup>, Caterina C Kaffes<sup>2</sup>, M Waleed Gaber<sup>2</sup>, Susan M Blaney<sup>2</sup> & Jennifer L West\*<sup>1</sup>

<sup>1</sup>Department of Bioengineering, Rice University, 6100 Main Street, MS-142, Houston, TX 77005, USA

<sup>2</sup>Texas Children's Cancer Center, Department of Pediatrics, Baylor College of Medicine, Houston, TX 77030, USA

\*Author for correspondence:

Tel.: +1 713 348 5955

Fax: +1 713 348 5877

[jwest@rice.edu](mailto:jwest@rice.edu)

Angiogenesis plays a critical role in tumor progression, and gliomas are among the most densely vascularized tumors. Consequently, there has been a surge in the number of antiangiogenic therapies available for glioma [1]. We previously proved that nanoshell (NS)-mediated photothermal therapy (PTT) improves survival time in a subcutaneous glioma model [2], and here, we apply targeted PTT to disrupt vasculature in orthotopic gliomas because this approach is simple, minimally invasive and should have limited side effects. In PTT, exposure to near-infrared light causes gold-based nanoparticles within a tumor to produce heat sufficient to induce cell death through mechanisms such as protein denaturation and cellular membrane rupture [3,4]. While this approach has previously been aimed directly towards cancerous cells, here we apply PTT to destroy endothelial cells forming tumor vessels via the same mechanisms of action. Killing the endothelial cells should inhibit vessel functionality, reducing the blood supply to the tumor. This physical disruption of angiogenesis should be less susceptible to the cellular escape mechanisms that have plagued other therapies. For example, gliomas treated with monoclonal antibodies upregulate cytokines and endothelial cell survival factors such as PDGF/PDGF receptor- $\beta$  and Ang-1/Tie2 [5], and undergo a metabolic switch toward glycolysis that promotes further invasion of tumor

cells into the normal brain [6]. Disruption of vessels with PTT should avoid such resistance. To date, nanoparticles explored for PTT include silica core/gold-shell nanoparticles (NSs) [7,8], hollow-gold nanospheres [9], nanorods [10,11], gold-gold sulfide nanoparticles [12,13], nanocages [14], copper sulfide nanoparticles [15,16] and gold spheres [17]. NSs were chosen for this work because they are simple to fabricate, contain a biologically inert gold surface that is readily available for conjugation to desired biomolecules and have a high per-particle photothermal transduction cross-section [18].

In the process of tumorigenesis, genetic alterations within cancer cells often induce upregulation of cell surface receptors; these 'molecular markers' distinguish diseased tissue from normal tissue, enabling targeted therapies. Nanoparticles have been coated with antibodies [19,20], aptamers [21], or peptides [9] to direct them toward specific tumor cell populations with unique surface markers upon extravasation from the bloodstream. However, areas of increased vascular permeability are spatially nonuniform in tumors, leading to irregular blood flow and high interstitial pressures that hinder the delivery of these agents to the tumor interstitial space via the 'enhanced permeability and retention effect' [22]. Targeting markers selective for tumor vessels avoids delivery difficulties since luminal endothelial cells are readily accessible to

circulating compounds and tissue penetration is not required for the therapeutic agent to reach its target [23]. This accessibility is particularly important for gliomas, since difficulty crossing the blood–brain barrier has limited the efficacy of many therapies. Potential targets for vascular-focused therapies include  $\alpha v$  integrins and angiogenic growth factors and their ligands [24]. For example, arginine–glycine–aspartic acid (which binds  $\alpha v\beta 3$ ) has been used to address both liposomal doxorubicin [25] and gold nanorods [26]. We chose to direct NSs toward tumor vessels by coating them with VEGF because this ligand and its receptors are the most important for glioma angiogenesis and have thus received the most focus among developing therapeutics [27,28]. VEGF is a tumor-secreted cytokine that exerts its effect by interacting with the transmembrane tyrosine kinase receptors VEGF receptor-1 (VEGFR-1) and VEGFR-2, which is highly expressed in glioma endothelium [29].

Here we describe the development of NS-mediated vascular-targeted PTT, which disrupts glioma vasculature with heat-based mechanisms so subsequent reductions in nutrient and oxygen transport result in tumor necrosis. NSs were coated with VEGF<sub>165</sub>, the most common isoform of VEGF, and *in vitro* studies verified that these NSs can bind to VEGFR-2-positive endothelial cells at levels sufficient for photothermal ablation. Subsequent *in vivo* work was performed using intracerebral U373 human glioma tumors. Coating NSs with VEGF nearly doubled the proportion of NSs bound to tumor vessels. For therapy experiments, laser light was applied through a glass cranial window, which not only enabled light delivery to the tumor but also allowed changes in tumor-associated vasculature to be monitored by intravital microscopy. Examination of intravital microscopy images and histology specimens revealed that therapy disrupted tumor vessels while leaving the normal brain unharmed, suggesting that this treatment strategy could be a valuable alternative to conventional antiangiogenic brain tumor therapy in the future.

## Materials & methods

### ■ NS preparation & characterization

NSs with spherical silica cores and thin gold shells were prepared as described previously [2,30] and characterized by UV-visible spectroscopy (Cary50 Bio, Varian, CA, USA) and scanning electron microscopy (FEI Quanta 400). To link NSs to VEGF, orthopyridyl disulfide (OPSS)–polyethylene glycol (PEG)–*N*-hydroxysuccinimide

(NHS; 2 kDa, Creative PEGWorks, NC, USA) was reacted with murine VEGF<sub>165</sub> (PeproTech, NJ, USA) at a 10:1 molar ratio (ten PEG moieties per VEGF molecule) at 4°C overnight. Conjugation was confirmed via silver staining on proteins separated by polyacrylamide gel electrophoresis (4–15% Tris-HCl precast gels and silver stain from Bio-Rad, CA, USA). The OPSS–PEG–VEGF then reacted for 1 h at 4°C with NSs suspended in milli-Q water ( $4 \times 10^9$  NS/ml) to produce VEGF-coated NSs (VEGF-NS); this reaction included 1200 VEGF proteins per NS. Next, nine parts NSs were incubated with one part 25  $\mu$ M methoxy PEG-thiol (5 kDa, Laysan Bio, AL, USA) overnight at 4°C. Control NSs were also prepared with only methoxy PEG-thiol (PEG-NS). After VEGF and/or PEG modification, NSs for *in vitro* studies were centrifuged and suspended in cell culture medium; NSs for *in vivo* studies were concentrated via cross-flow filtration (11 cm<sup>2</sup> polysulfone filters, 0.05  $\mu$ m molecular weight cut-off, Spectrum Laboratories, Inc., CA, USA) and suspended in sterile phosphate-buffered saline (PBS).

To confirm and quantify the presence of VEGF on NSs, dynamic light scattering, zeta potential measurements, and a solution-based ELISA were performed. For the ELISA, NSs were incubated with 10  $\mu$ g/ml rabbit antimouse VEGF (PeproTech), then with 20  $\mu$ g/ml Horseradish peroxidase (HRP)-conjugated antirabbit IgG (Sigma). Nonspecific reaction sites were blocked with 3% bovine serum albumin (Sigma) in PBS. To remove unbound antibodies, NSs were centrifuged twice (500 g, 5 min) and suspended in 3% bovine serum albumin. Bound HRP was developed with 3,3',5,5'-tetramethylbenzidine dihydrochloride (Sigma) for 15 min and the reaction was stopped by adding 2 M sulfuric acid. Developed HRP was compared with a standard curve of the HRP-labeled anti-IgG by measuring the absorbance at 450 nm. The number of antibodies per nanoparticle was calculated by dividing the number of peroxidase-labeled anti-IgG moieties by the number of NSs in solution.

Further NS characterization provided in the SUPPLEMENTARY INFORMATION (see online: [www.futuremedicine.com/doi/suppl/10.2217/nnm.11.189](http://www.futuremedicine.com/doi/suppl/10.2217/nnm.11.189)) includes a transmission electron micrograph, the heating profile of NSs in suspension and the optical extinction spectra before and after surface functionalization. In addition, the stability of the conjugated NSs was verified by spectroscopically monitoring optical extinction versus time after introducing the nanoparticles into a 1% saline solution, which mimics physiological

ionic conditions. Reduction of peak absorbance over time indicates nanoparticle aggregation; conversely, peak maintenance confirms stability. Both the PEG- and VEGF-coated NSs were extremely stable compared with bare NSs, indicating that the conjugates should remain intact once injected into animals.

#### ■ *In vitro* assessment of vascular-targeted PTT

*In vitro* tests were performed to confirm that VEGF-NS could bind VEGFR-2 positive cells and facilitate thermal ablation of these targeted cells. Mile Sven 1 (MS1) murine endothelial cells were obtained from the American Type Culture Collection and cultured in DMEM supplemented with 10% fetal bovine serum and 1% L-glutamine, penicillin and streptomycin. These cells were chosen to mimic VEGFR-2-positive endothelial cells lining tumor vasculature, which is the target of this therapy. Cells grown in chambered coverglass received 1 ml of saline, PEG-NS ( $1.1 \times 10^{10}$  NS/ml) or VEGF-NS ( $1.1 \times 10^{10}$  NS/ml). After rinsing three times to remove unbound NSs, an 808-nm laser was applied ( $60 \text{ W/cm}^2$ , 3 min). Following 1-h incubation, samples were stained with 1  $\mu\text{M}$  calcein AM and 4  $\mu\text{M}$  ethidium homodimer-1 (Live/Dead<sup>®</sup> staining kit, Molecular Probes, OR, USA) and fluorescence microscopy was performed with an inverted Zeiss Axiovert 135 phase contrast microscope (Carl Zeiss, NJ, USA) to investigate cell viability. Samples were also imaged with a darkfield microscopy adaptor (Cytoviva, AL, USA) on the same microscope to assess NS binding to the cells.

#### ■ Tumor inoculation

*In vivo* models were used to evaluate NS accumulation in intracranial tumors and to confirm the ability to disrupt tumor vasculature with PTT. All animals were used under an approved protocol of the Institutional Animal Care and Use Committee (IACUC) of the Baylor College of Medicine (TX, USA). U373 human high-grade glioma cells were engineered to constitutively express both firefly luciferase and green fluorescent protein (GFP) as described previously [2,31] and cultured in RPMI 1640 medium (Invitrogen, CA, USA) supplemented with 1% glutamine and 10% fetal bovine serum. Cells were detached from flasks with trypsin-EDTA and diluted in culture medium to  $5 \times 10^7$  cells/ml for inoculation into male IcrTac:ICR-PrkdcSCID mice (a spontaneous mutant model deficient in T and B cells; Taconic Farms, NY, USA). In all mice,

$10^5$  cells were injected with a Hamilton syringe 1 mm lateral right to the middle sagittal suture, 2 mm anterior of the lambdoid suture and 3 mm below the surface of the brain.

For the biodistribution study, a 0.8-mm diameter Burr hole was created in the skull with a microsurgical drill to allow cell implantation. By contrast, for treatment studies the tumors were implanted using the cranial window procedure of Gaber *et al.*, published in detail elsewhere [32]. This approach places a 4–5-mm width/length glass window over the tumor, enabling laser light to be delivered to the tumor and allowing changes in the tumor to be monitored with intravital microscopy. Before tumor implantation surgery, each mouse was anesthetized with 50 mg/kg Nembutal<sup>®</sup> (sodium pentobarbital) and the surgical area cleaned with alcohol and Betadine<sup>®</sup>. After surgery, the mice received buprenorphine intraperitoneally (Buprenex<sup>®</sup>, 0.2 mg/kg) every 12 h for 2 days to minimize pain as well as antibiotics in their water for 5 days to prevent infection (1.7 ml Baytril<sup>®</sup> 100 [enrofloxacin, 100 mg/ml] per 400 ml H<sub>2</sub>O). Tumor growth was monitored *in vivo* at predetermined time-points with intravital microscopy or bioluminescent imaging to observe the GFP signal and luciferase activity, respectively. For bioluminescent imaging, isoflurane-anesthetized animals were imaged with a Xenogen IVIS<sup>®</sup> 100 (Caliper Life Sciences, CA, USA) 10 min after receiving intraperitoneal injections of 150 mg/kg D-luciferin (Xenogen), which emits light when oxidized in the presence of luciferase and ATP. In preliminary studies we established tumor growth curves by comparing signal intensity with histological samples acquired on various days post cell implantation. These pre-established growth curves allowed us to estimate when tumor diameter had reached 3–5 mm based on both the bioluminescent signal and the number of days since tumor implantation.

#### ■ Analysis of NS distribution in mice bearing intracerebral glioma tumors

For the biodistribution study, mice received PEG-NS or VEGF-NS intravenously (100  $\mu\text{l}$ ,  $1.7 \times 10^{10}$  NSs) when the tumor diameter reached 3–5 mm. After waiting 6, 24 or 48 h, the mice were euthanized and the spleen, liver, blood, kidney, heart, tumor and normal brain were collected. Each specimen (apart from blood) was divided into two pieces – one for histology and one for quantitative analysis of gold content by inductively coupled plasma–mass spectrometry (ICP–MS). Blood was only analyzed by ICP–MS.

Three mice were used per group per time-point, for a total of 18 mice. These numbers were chosen based on our previous experience studying PTT in murine glioblastoma models, with the goal of using as few animals as possible while maintaining the ability to gather scientifically valid data.

ICP-MS is a common method for analyzing gold content in tissue and its utility has previously been demonstrated with spheres [33], NSs [2] and nanorods [34]. Tissue samples for ICP-MS were lyophilized, weighed and digested with 0.5 ml aqua regia for 48 h. Trace grade nitric acid and hydrochloric acid were purchased from Sigma-Aldrich and VWR, respectively. Digested samples were further diluted with 1% aqua regia and filtered through a 0.45- $\mu$ m filter. Standard solutions of known gold concentrations were prepared in 1% aqua regia using certified reference material Gold Standard for ICP (Sigma-Aldrich). Standards and samples were analyzed for 197Au with germanium as an internal standard using the ELAN<sup>®</sup> 9000 ICP-MS from Perkin-Elmer (MA, USA).

Histological specimens were formalin-fixed, paraffin embedded, cut into 6- $\mu$ m sections and fluorescently labeled to show blood vessels. Samples were incubated in xylene twice for 10 min before hydrating through a series of alcohol (100, 90, 70 and 50%; 3 min each) and water (5 min). Antigen retrieval was accomplished by incubating slides in proteinase K (10  $\mu$ g/ml, at 37°C for 15 min) and slides were cooled with running water for 3 min. After rinsing with PBS containing 0.1% Tween<sup>®</sup> 20, nonspecific binding sites were blocked with 10% donkey serum in PBS for 45 min. Samples then reacted with goat antimouse CD31 (15  $\mu$ g/ml, R&D Systems) overnight at 4°C. Three rinses with PBS containing 0.1% Tween 20 were performed before exposing samples to AlexaFluor 488-conjugated donkey antigoat IgG (10  $\mu$ g/ml, Invitrogen) for 1 h. Rinsed sections were mounted with Vectashield<sup>®</sup> containing 4',6-diamidino-2-phenylindole. To evaluate the proximity of NSs to blood vessels, dual darkfield and fluorescence microscopy were performed on stained tissue sections using a Cytoviva<sup>®</sup> adaptor attached to a Zeiss Axiovert 135 inverted microscope. With darkfield microscopy, indirect sample illumination allows NSs to be visualized against the tissue background due to their enhanced light scattering properties [2]. The nanoparticle signal from each darkfield image was merged with a fluorescence image from the same field of view to qualitatively assess NS proximity to blood vessels. NS distance from the nearest blood vessel

was quantified to establish whether coating NSs with VEGF increased their adherence to blood vessels compared with NSs coated with PEG (image processing and analysis details are in the SUPPLEMENTARY INFORMATION).

### ■ PTT of intracerebral glioma tumors

For PTT, mice received 150  $\mu$ l saline or NSs through the tail vein ( $2.9 \times 10^{11}$  NS/ml) and 24 h later the 808-nm laser was applied through the cranial window (6 W/cm<sup>2</sup>; ~4.5 mm beam diameter; 3 min). Three mice each received PEG-NS, VEGF-NS or saline. Response to treatment was monitored with intravital microscopy and bioluminescence imaging. Mice were euthanized according to Baylor's IACUC criteria. The experiment was repeated twice to ensure reproducibility of the data.

To quantify changes in vasculature induced by treatment, intravital microscopy images acquired on the day of laser application and 3 days later were analyzed for the three mice that received VEGF-NS and the three mice that received saline. Mice that received PEG-NS could not be included in the analysis since only one mouse survived in the 3 days; it remains to be investigated in future studies why the mice treated with PEG-NS did not survive longer. For the analysis, vessels within 1.5 mm from the tumor center were traced in ImageJ software (NIH), filled, and the image binarized (SUPPLEMENTARY INFORMATION). Vessel density was calculated as the area of positive pixels divided by the total area and the density on day 3 was normalized to the density on day 0 to quantify treatment effect. Lastly, treatment effect was also monitored with histology. A subset of mice were euthanized immediately following laser exposure and the brain tissue was excised for hematoxylin and eosin staining. These samples were examined to determine the effects of therapy on both the tumor and the normal brain.

## Results

### ■ NS characterization

Scanning electron microscopy indicated that the NSs had a homogeneous size distribution (FIGURE 1A). Silver staining of PEG-VEGF protein samples separated by SDS-PAGE confirmed the conjugation of VEGF to OPSS-PEG-NHS. As shown in FIGURE 1B, addition of OPSS-PEG-NHS increased the observed molecular weight, with several bands appearing based on the number of PEG chains added. VEGF appears as a 19 kDa monomer due to reducing conditions used to prepare the gel. For the biodistribution

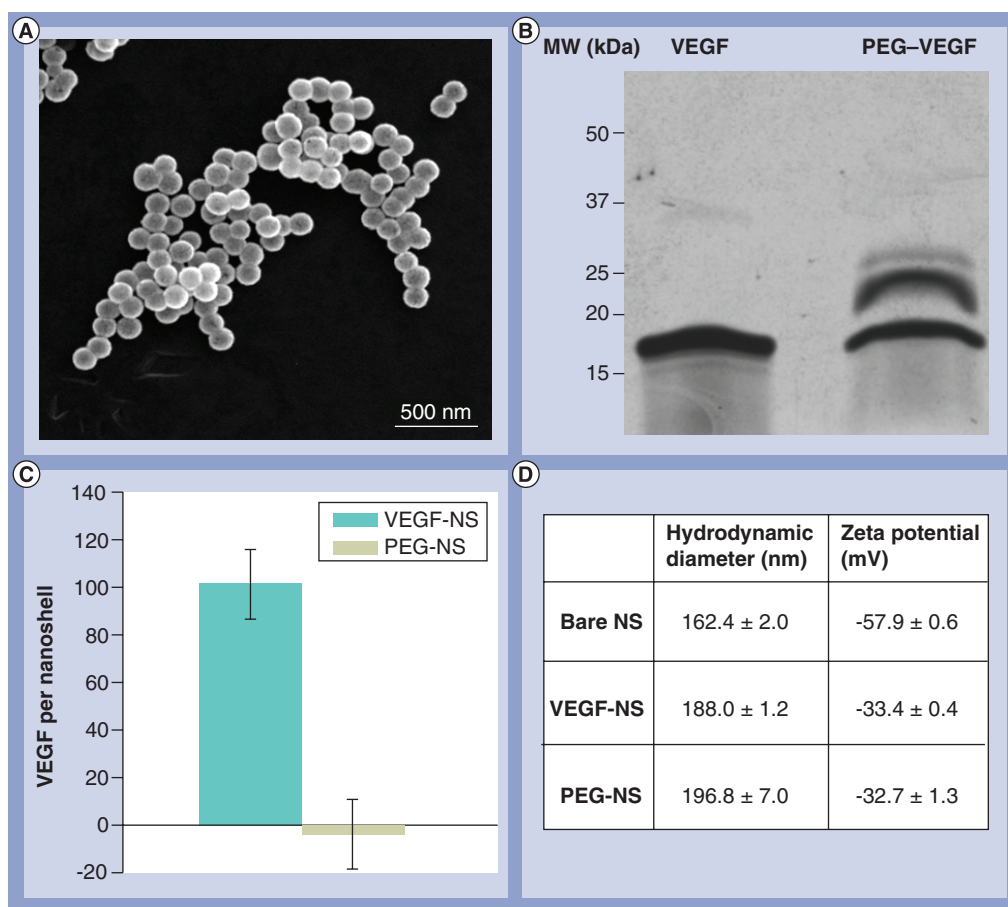


**Figure 1. Nanoshell characterization.** (A) Scanning electron microscopy confirmed nanoshells had a uniform size distribution. (B) Silver staining of proteins separated by gel electrophoresis confirmed VEGF conjugation to orthopyridyl disulfide-PEG-*N*-hydroxysuccinimide (2000 Da), with different bands of increased molecular weight appearing based on the number of PEG chains attached. (C) An ELISA revealed approximately 100 VEGF molecules bound to each NS; background on PEG-NS controls was minimal. (D) Upon functionalization, nanoparticle hydrodynamic diameter increased and zeta-potential magnitude decreased. NS: Nanoshell; PEG: Polyethylene glycol; PEG-NS: Polyethylene glycol-coated nanoshells; VEGF-NS: VEGF-coated nanoshells.

study, NSs were characterized with the ELISA, which showed  $100.9 \pm 14.3$  VEGF per NS; PEG-NS controls showed minimal background ( $-3.9 \pm 14.0$ ) (FIGURE 1C). For the therapy study, the NSs were characterized further with dynamic light scattering and zeta potential measurements, which confirmed increased hydrodynamic diameter and neutralized surface charge upon functionalization, respectively (FIGURE 1D). Results of further characterization are displayed in SUPPLEMENTARY FIGURE 1.

#### ■ VEGF-conjugated NSs bind murine endothelial cells *in vitro* to facilitate PTT

The ability of VEGF-NS to bind murine endothelial cells that overexpress VEGFR-2 and facilitate thermal therapy was first tested *in vitro*. Darkfield microscopy confirmed that VEGF-NS

could bind MS1 cells, while PEG-NS could not bind the cells and were thus removed during the rinsing steps (FIGURE 2A). NSs appear red under darkfield microscopy due to their enhanced light-scattering properties. Upon near-infrared-irradiation, only MS1 cells that had been exposed to targeted (VEGF-coated) NSs experienced loss in viability, indicated by red ethidium homodimer-1 fluorescence (FIGURE 2B). Comparatively, cells previously exposed to saline or PEG-NS remained viable (green calcein acetoxyethyl ester fluorescence).

#### ■ VEGF- & PEG-NSs accumulate in intracerebral tumors

After the initial *in vitro* assessment of vascular-targeted PTT, a biodistribution study was performed. Using ICP-MS, the mean and standard deviation of gold content in several organs

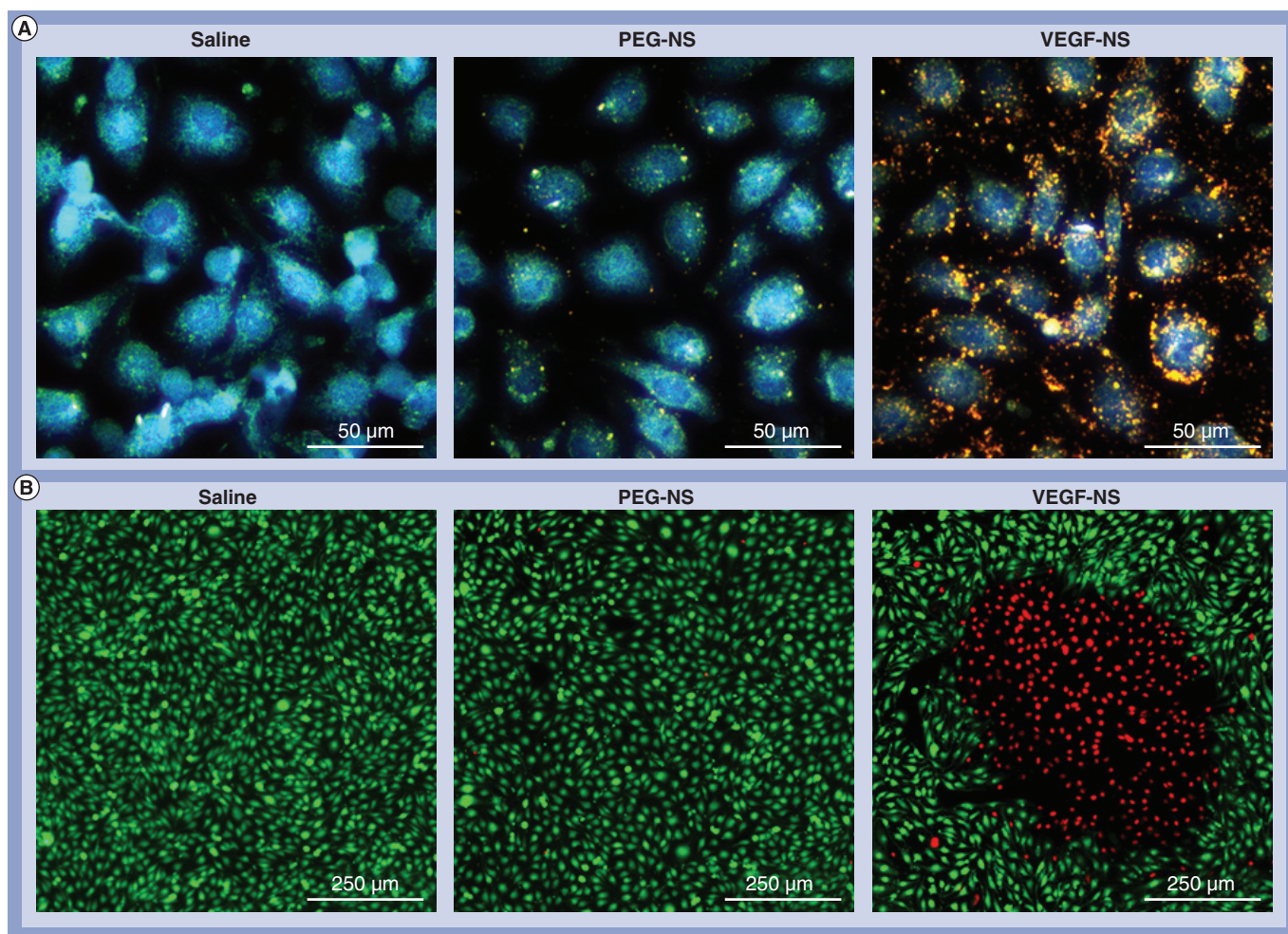


**Figure 2.** *In vitro* assessment of photothermal therapy mediated by VEGF-coated nanoshells. M1 endothelial cells that overexpress VEGF receptor (VEGFR-2) were incubated with saline, PEG-NS or VEGF-NS prior to darkfield microscopy and 808-nm laser irradiation (6 W/cm<sup>2</sup>, 3 min). **(A)** Darkfield microscopy proves that VEGF-NS bind M1 cells that express VEGFR-2, while PEG-NS do not. NSs appear red against the blue cell background. **(B)** Fluorescence microscopy reveals that only cells targeted with VEGF-NSs experience loss in viability upon laser irradiation. Live cells fluoresce green (calcein acetoxyethyl ester) and dead cells fluoresce red (ethidium homodimer-1).

PEG-NS: Polyethylene glycol-coated nanoshells; VEGF-NS: VEGF-coated nanoshells.

were calculated from three mice per group after NSs circulated 6, 24 and 48 h (FIGURE 3A & SUPPLEMENTARY TABLE 1). Organs analyzed included the spleen, liver, kidney, blood, heart, tumor and brain. The kidney and heart were included since antivasular therapies, such as bevacizumab, have been linked to proteinuria and hypertension [35]. Coating (PEG or VEGF) did not greatly influence nanoparticle accumulation in the kidney; however, more gold was found in the heart and liver and less in the spleen when the particles were coated with VEGF. In addition, NSs coated with VEGF were cleared more rapidly from the blood than those coated with PEG.

FIGURE 3B shows an expanded y-axis for tumor and normal brain samples. Differences between samples were tested for significance using a one-way analysis of variance with *post hoc* Tukey and

samples with  $p < 0.05$  are marked in FIGURE 3B. This analysis did not reveal any difference in gold accumulation in the tumor at any given time based on NS coating (VEGF or PEG). To provide a normalized comparison of PEG-NS versus VEGF-NS, the gold content in the tumor was divided by the content in the brain and in the blood to account for background distribution. At 6 h, the tumor-to-brain gold content ratio was 7.0 for VEGF-NS and 2.8 for PEG-NS, and the tumor-to-blood ratio was 2.2 for VEGF-NS versus 0.03 for PEG-NS. While this suggested the VEGF-NS amass more rapidly in the tumor, over time the ratios equalized at approximately 15-times more gold in the tumor than the normal brain and ten-times more gold in the tumor than in the blood. Comparison of normalized data with a student's t-test revealed no statistically

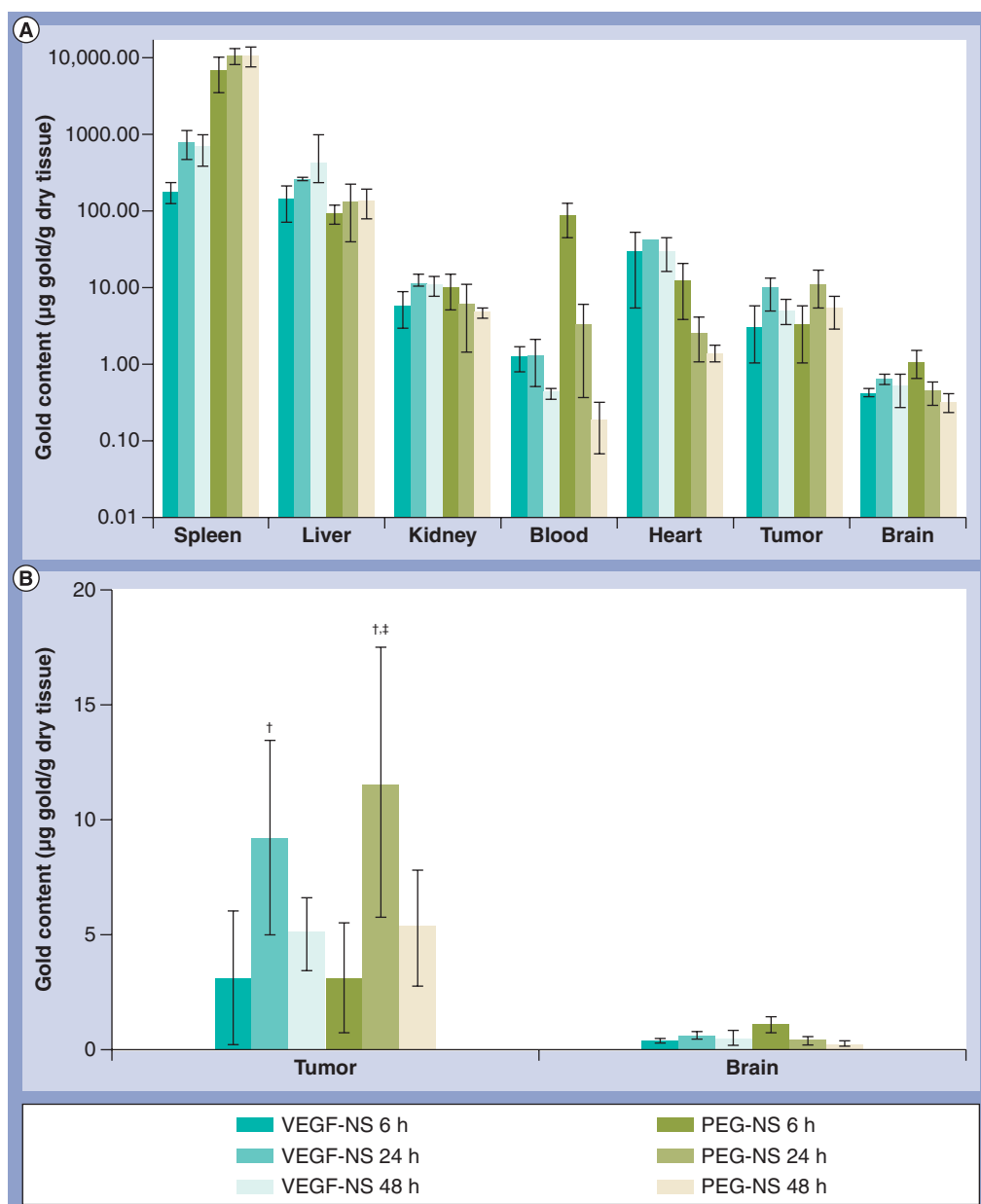


**Figure 3. Distribution of VEGF-coated and polyethylene glycol-coated nanoshells in mice with intracerebral tumors. (A)** Gold content in various organs was determined by inductively coupled plasma–mass spectrometry. Data depicts mean  $\pm$  standard deviation. No standard deviation is shown for the heart in the VEGF-NS group at 24 h because  $n = 2$  in this group. **(B)** Nanoshell distribution to the tumor and normal brain is shown with an expanded y-axis. †Significant versus all normal brain groups. †‡Significant versus both 6-h tumor groups; analysis of variance with *post hoc* Tukey. PEG-NS: Polyethylene glycol-coated nanoshells; VEGF-NS: VEGF-coated nanoshells.

significant differences at any time-point, again indicating that coating did not greatly influence the total number of NSs delivered to the tumor. Importantly, regardless of coating, more NSs were found in the tumor than in the normal brain at all times. This difference was maximized at 24 h, rendering it the best time to apply the laser to minimize the potential for off-target effects. Darkfield and fluorescence microscopy

of all tissue acquired 24 h post-NS injection visually confirmed the ICP–MS data (FIGURE 4). For example, the darkfield images reveal fewer VEGF-NS in the spleen and more in the liver than PEG-NS. In the fluorescence images, vessels are green (anti-CD31) and nuclei are blue (4',6'-diamidino-2-phenylindole), and within all organs both NS types remain in close proximity to vasculature.

To more stringently evaluate the effect of VEGF targeting on NS intratumoral localization, the distance of each NS from the nearest tumor vessel was determined by merging images showing the NSs' positions (determined from darkfield microscopy) with fluorescence images from the same field of view (SUPPLEMENTARY FIGURES 2–6). FIGURE 5 shows three representative areas for VEGF-NS (FIGURE 5A) and PEG-NS (FIGURE 5B). The VEGF-NS appear to remain closer to tumor vessels than the PEG-NS, and quantitative analysis confirmed this result (FIGURE 5C). For the analysis, an investigator blinded to the treatment groups counted the number of NSs within vessels (the region  $<0\ \mu\text{m}$ ) and within distinct regions  $5\ \mu\text{m}$  wide outside the vessels. These were converted to percentages by dividing the number of NSs in each region by the number in each image, and the results were averaged across six images (total analysis of 271 PEG-NS and 215 VEGF-NS). A one-way analysis of variance with *post hoc* Tukey revealed that statistically significantly more VEGF-NS adhered to or remained within the vessels (the region  $<0\ \mu\text{m}$ ) than PEG-NS ( $p = 0.00002$ ). Specifically, 59.2% of VEGF-NS remained adherent to/within vessels, while only 31.6% of PEG-NS remained adherent to/within vessels. Furthermore, there were significantly more VEGF-NSs within vessels (the region  $<0\ \mu\text{m}$ ) than within any region outside vessels (regions  $>0\ \mu\text{m}$ ;  $p < 5 \times 10^{-8}$  for all). By comparison, the percentage of PEG-NSs within vessels only differed significantly from the percentage of PEG-NSs in regions beyond  $10\ \mu\text{m}$  from the vessels ( $p < 0.005$ ). Together, these data prove the VEGF coating allows NSs to bind their target receptors on vascular endothelial cells *in vivo*.

#### ■ Intravital microscopy & histology indicate that NS-mediated PTT can disrupt tumor-associated vasculature

To evaluate the effects of therapy on the tumor and the normal brain, the laser was applied 24 h postintravenous injection of NSs. In this case, a higher NS dose was delivered ( $4.35 \times 10^{10}$  NSs per mouse) with the prediction that more nanoparticles would accumulate in the tumor, enabling more effective treatment. Response to treatment was monitored with intravital microscopy and histology.

With intravital microscopy the superficial layer of the tumor appears as a bright region due to the GFP signal emitting from the tumor cells and the tumor-associated vessels are observed

as shadows. This allows changes in vasculature induced by therapy to be monitored both qualitatively and quantitatively by calculating vessel density. FIGURE 6A shows intravital microscopy images acquired for a mouse that received saline and for a mouse that received VEGF-NS 1 day prior to laser treatment. The left column displays an image acquired immediately before the laser was applied and the right column displays the same region 6 days later. In the saline control mouse, the GFP signal indicates rapid tumor growth over time and the vessels appear to be maturing. By contrast, the vessels are disrupted following treatment for the VEGF-NS treated mouse and the GFP signal indicates a reduced rate of tumor growth.

To quantify changes in vasculature induced by treatment, intravital microscopy images acquired on the day of laser application (day 0) and 3 days later were analyzed for three mice that received VEGF-NS and three mice that received saline. Vessels within  $1.5\ \text{mm}$  from the tumor center were traced in ImageJ software, filled, and the image binarized (SUPPLEMENTARY FIGURE 7). Vessel density was calculated as the area of positive pixels divided by the total area and the density on day 3 was normalized to the density on day 0. As shown in FIGURE 6B, vessel density increased by 18% for the saline group but decreased by 24% for the VEGF-NS treatment group over these three days ( $p = 0.025$ , student's *t*-test). Data in the figure represent the mean and standard error for each group.

Lastly, treatment effect was also monitored with histology. A subset of mice was euthanized immediately following laser exposure and tissue was excised to determine the effects of therapy on both the tumor and the normal brain since the light encountered both regions after it passed through the cranial window. FIGURE 7 displays images of hematoxylin and eosin stained sections of the tumor, the normal brain and the interface between the two regions for mice exposed to saline, PEG-NS and VEGF-NS. There were no changes in the vasculature in the normal brain for any group, indicating that both laser power and nanoparticle concentration in this region were low enough to prevent thermal damage. By contrast, distinct treatment effects (such as vessel dilation and hemorrhaging; bright pink areas in the images) were observed in the tumor vasculature for both PEG-NS- and VEGF-NS-treated mice, but not for saline control mice. Interestingly, at the tumor periphery, where vessel density (and thus NS concentration)

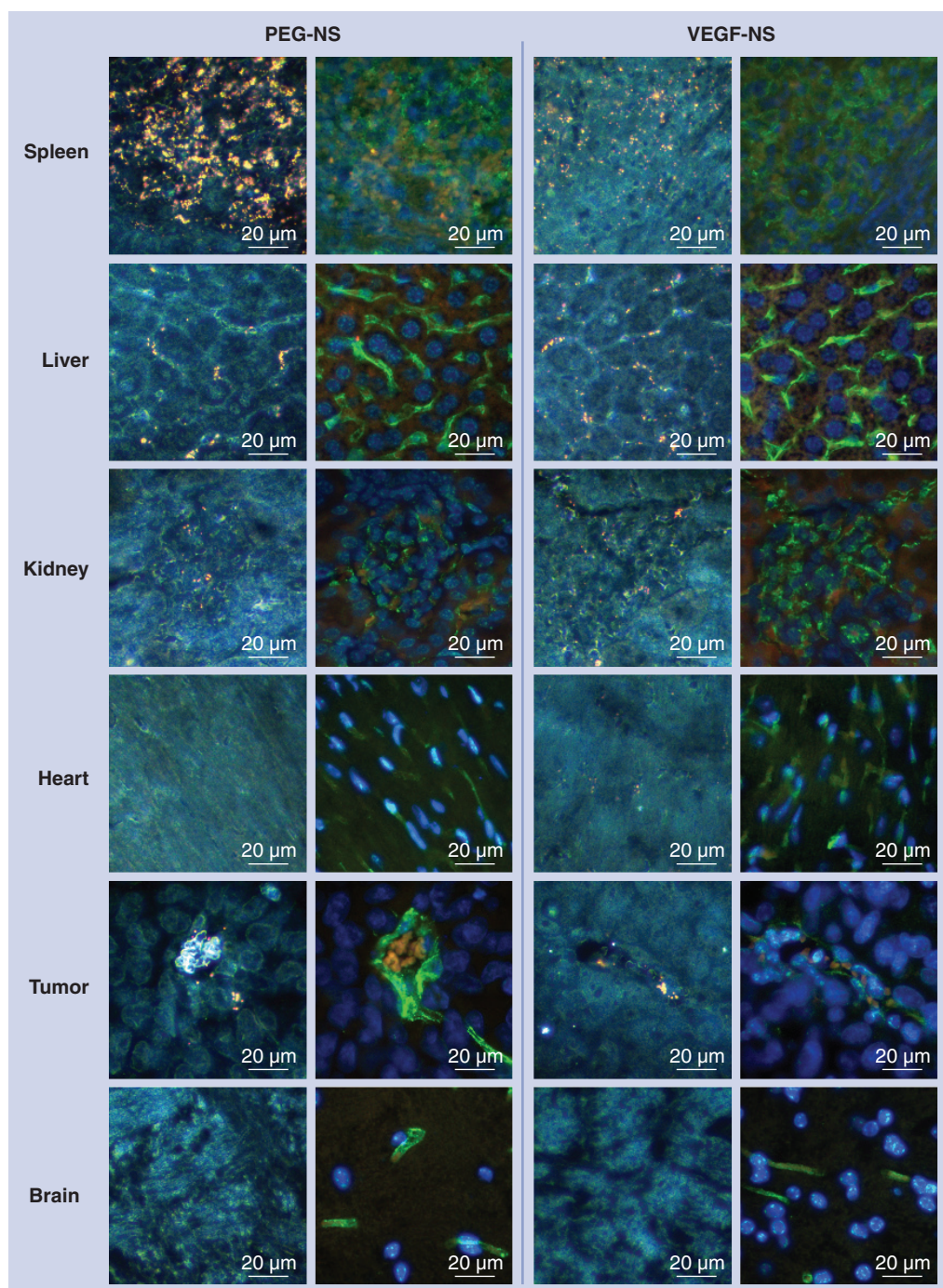


**Figure 4. Visualization of nanoshell distribution.** Accumulation of PEG-NS and VEGF-NS in various organs was observed with darkfield microscopy (columns one and three). Fluorescence images (columns two and four) from the same fields of view show CD31 (green), nuclei (blue), and some tissue autofluorescence (orange). Generally, nanoshells are found in close proximity to blood vessels.

PEG-NS: Polyethylene glycol-coated nanoshells; VEGF-NS: VEGF-coated nanoshells.

is higher, the thermal damage was more pronounced. Importantly, this damage was confined to the tumor and did not spread beyond 500  $\mu\text{m}$  into the adjacent brain.

Ultimately, the mice treated with VEGF-NS experienced a 2.2-fold increase in median survival versus mice treated with saline, and

a similar 2.7-fold increase was observed upon repeating this study. While these initial data are worth noting given the aggressive nature of glioblastoma, we plan to perform survival studies with larger animal numbers in the future so that we can more thoroughly compare treatment outcomes with statistical analysis.

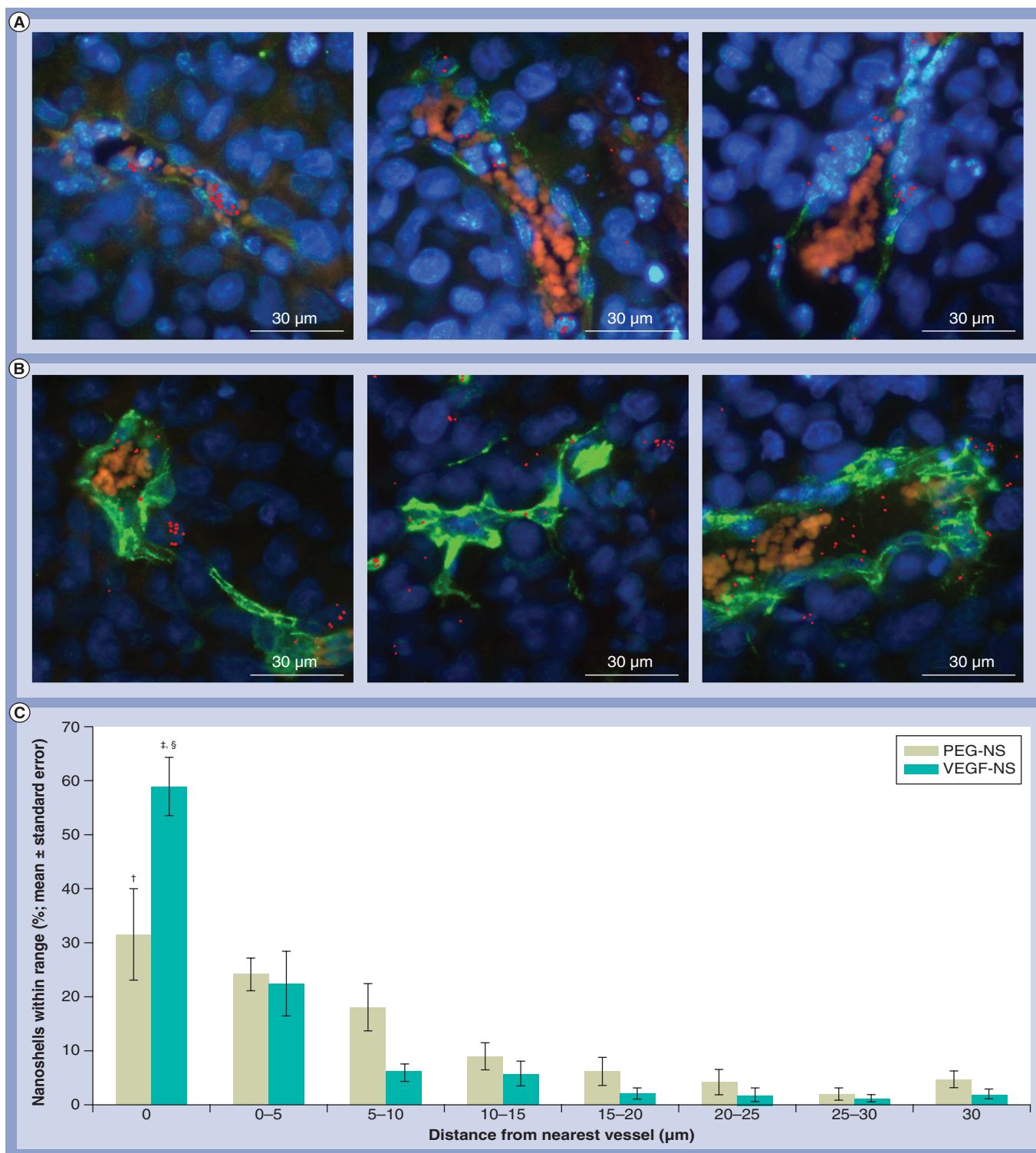


**Figure 5. Assessment of nanoshell proximity to tumor vasculature. (A & B)** To evaluate the targeting effect, images of nanoshells (red, derived from darkfield microscopy) were merged with fluorescence images from the same region in the tumor. Three representative areas, in which nuclei are blue (4',6-diamidino-2-phenylindole), endothelial cells are green (CD31), and red blood cells are orange (autofluorescence) are shown for **(A)** VEGF-NSs and **(B)** PEG-NSs. Generally, VEGF-NSs remain closer to vessels than PEG-NSs.

**(C)** Quantification of nanoshell distance from blood vessels confirmed that targeting with VEGF increased the adherence of nanoshells to tumor vessels.

<sup>†</sup>Significant versus PEG-NS >10  $\mu\text{m}$ ; analysis of variance with *post hoc* Tukey.

<sup>‡</sup>Significant versus PEG-NS <0  $\mu\text{m}$ .

<sup>§</sup>Significant versus VEGF-NS >0  $\mu\text{m}$ .

PEG-NS: Polyethylene glycol-coated nanoshells; VEGF-NS: VEGF-coated nanoshells.

## Discussion

Since the concept that tumors are angiogenesis-dependent was introduced in the 1970s [36], there has been explosive growth in the development of vascular-targeted cancer therapies. Antiangiogenic therapy is particularly well suited for high-grade gliomas because they are among the most densely vascularized tumors. Unfortunately, approaches that utilize antibodies or small molecule inhibitors to disrupt tumor vasculature have faced clinical setbacks, including toxicities and the inability to prevent cells from developing resistance mechanisms such as signaling through alternative pathways. To overcome these limitations, nanoparticle-mediated therapies are now being investigated. Here, VEGF-coated NSs were evaluated for their ability to target intracerebral gliomas and to facilitate subsequent vascular-focused PTT since the VEGF-R pathway is critical in glioma angiogenesis. This work provides an initial pre-clinical validation of vascular-targeted PTT, and our future work will refine the parameters of this therapy and confirm the data of this pilot work in large-scale studies with sample sizes determined by power analysis.

Vascular-targeting with NSs confers several advantages for PTT. First, because the

targeted receptor is expressed on the luminal endothelium, NSs do not need to extravasate out of blood vessels for therapy to be effective. Furthermore, the NSs do not need to evade the blood–brain barrier, which is disrupted in high-grade glioma but may not be disrupted in early-stage tumors. Second, the genetic and molecular changes that occur in tumor-associated endothelial cells are consistent across multiple tumor lineages, so VEGF-NS may be effective against several diseases besides glioma, increasing the applicability of this new therapy. In addition, endothelial cells are relatively genetically stable, and therefore, less likely to develop resistance than tumor cells [23]. Even if resistance to chemotherapy does develop, vascular-targeted PTT should remain effective provided target receptor expression is maintained. This hypothesis is based upon the demonstration that some drug-resistant breast cancer cells are susceptible to NS-mediated PTT [37]. A final advantage of vascular targeting specific to the VEGF ligand used in this work is based on the discovery that the VEGF-signaling pathway regulates both paracrine and autocrine promotion of glioma tumorigenesis [38]. Since VEGFR-2 is expressed on both endothelial cells and some brain tumor cells, VEGF-NS could potentially inhibit tumor

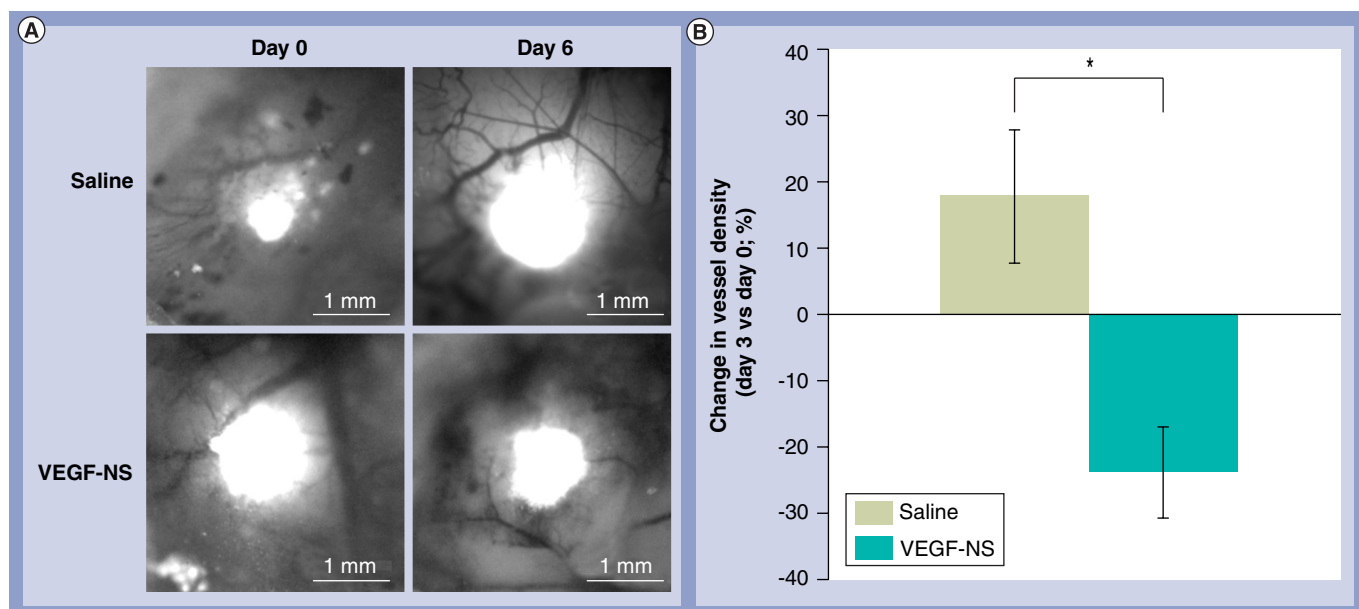


**Figure 6. Intravital microscopy reveals changes in tumor vasculature following treatment.** (A) Changes in tumor signal and vessel morphology were qualitatively evaluated by comparing intravital microscopy images acquired on the day the laser was applied and 6 days later. The mouse treated with saline shows increasing tumor signal and signs of vessel maturation, while the mouse treated with VEGF-NS shows a stable tumor signal and signs of vessel disruption. (B) Quantification of vessel density from intravital microscopy images highlights the treatment effect. Mice that received saline exhibited a mean increase in vessel density of 18% over 3 days after laser treatment (green bar) while mice that received VEGF-NS experienced a 24% decrease in vessel density (turquoise bar). Data show mean  $\pm$  standard error. These differences were significant at the 95% CI. \* $p = 0.025$ ; student's *t*-test. VEGF-NS: VEGF-coated nanoshells.

growth by enabling thermal ablation of both targets.

Vascular-targeted PTT was assessed *in vitro* and *in vivo*. *In vitro*, MS1 cells were used to model endothelial cells lining tumor vasculature. U373 cells were not used *in vitro* because they are tumor cells, and the goal of the targeting is to bind endothelial cells. NSs coated with VEGF bound to VEGFR-2 expressing endothelial cells *in vitro*, marking these cells for ablation upon exposure to near-infrared light. Treatment was subsequently studied further using an orthotopic tumor model, which is more clinically relevant than subcutaneous models since the microenvironment influences cancer cell behavior. In addition, the intracerebral tumor model allowed effects of therapy on the normal brain to be assessed; any new glioma treatment must minimize damage to the normal brain to provide

the best possible quality of life for patients following therapy. The U373 cell line was used to induce tumor growth *in vivo*, enabling generation of tumor-associated vessels that could be targeted by this therapy. *In vivo*, both PEG-NS and VEGF-NS accumulated at higher levels in intracerebral tumors than in the normal brain, and this delineation is necessary for therapy to be both effective and safe. Notably, similar to the results of others who have studied the effect of surface coating on nanoparticle distribution [39,40], we concluded that adding VEGF to NSs did not increase their accumulation in the tumor; however, it did increase their localization to the desired target, VEGFR-2 positive endothelial cells lining the tumor vessels, by nearly double. As a result, vessel disruption was achieved selectively in the tumor and at its periphery, but not in the adjacent normal brain of mice treated

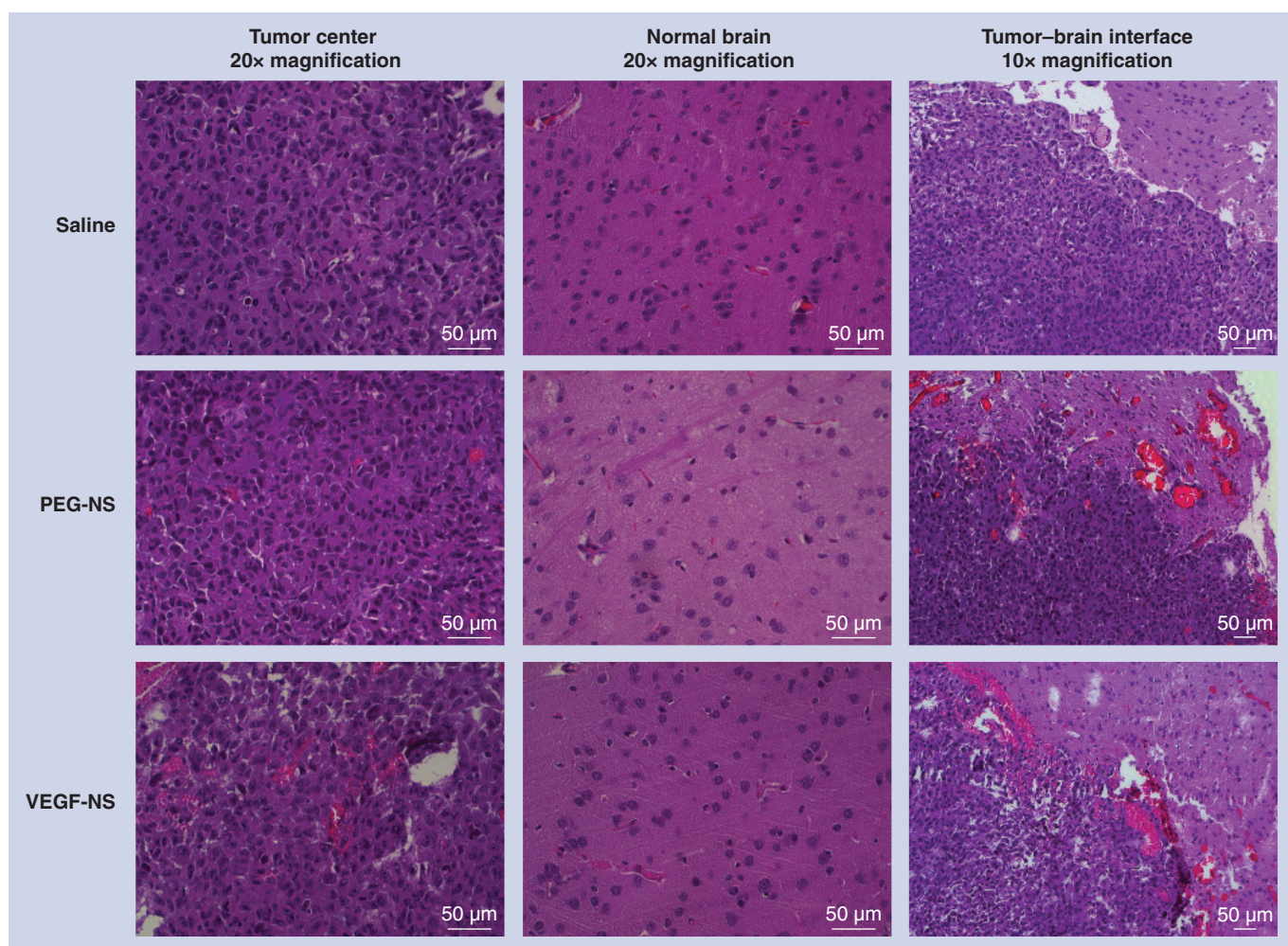


**Figure 7. Histological evaluation of vascular-targeted photothermal therapy.** Mice that received saline, PEG-NSs, or VEGF-NSs were sacrificed immediately after laser exposure to evaluate the effects of vascular-targeted photothermal therapy on the tumor and the normal brain with hematoxylin and eosin staining. No signs of thermal damage were observed in the normal brain for all groups nor in the tumor for mice exposed to saline. Comparatively, mice exposed to VEGF-NSs and PEG-NSs showed evidence of vessel dilation and hemorrhaging within the tumor.

with NSs and single-laser exposure. Similar effects were not observed in control mice. We believe future studies will confirm that this vascular disruption is sufficient to reduce the flow of nutrients and oxygen to the tumor and subsequently induce tumor necrosis. Furthermore, in future work we will critically assess the stability of the VEGF conjugates after they have been introduced *in vivo*. While gold–sulfur bond energies are strong and we have observed superior stability of these nanoparticles under physiological saline conditions (SUPPLEMENTARY INFORMATION), it remains to be proven whether or not the VEGF is displaced from the NSs *in vivo*.

In the future, it may be necessary to use a more direct mode of light delivery, such as a fiber-optic probe, to ensure more even distribution of light energy throughout the tumor, avoiding energy loss that occurs with external delivery as light traverses the normal brain before reaching the tumor, and prevent off-target heating of NSs that may accumulate in the normal brain. This may enable lower laser powers to be utilized to achieve the same therapeutic benefit. The feasibility of fiber-optic light delivery has already been demonstrated in two studies of nanoparticle-mediated therapy of brain tumors [41,42]. In the first, a probe delivered light for vascular-targeted photodynamic therapy of 9L glioma in rats and survival time was prolonged almost fourfold [41]. In the second, a probe delivered light for NS-mediated PTT of canine brain tumors [42]. Intratumoral temperatures of  $65.8 \pm 4.1^\circ\text{C}$  were achieved in the presence of nontargeted NSs while the maximum temperature in the normal brain was  $48.6 \pm 1.1^\circ\text{C}$ , below the damage threshold [42]. In future studies, it will be both interesting and important to determine whether the temperatures achieved in the tumor and the normal brain are influenced greatly by the changes in intratumoral NS localization induced by targeting the NSs to tumor vasculature with VEGF. In addition, it will be important to establish if this approach can capture tumor cells beyond the main tumor mass. Infiltrative glioma cells missed by conventional therapies are often responsible for patient relapse [43], so it is critical to develop PTT with the goal of eliminating these evasive cells. Tumor satellites typically form along the vascular supply, supporting the use of VEGF-coated NSs for glioma treatment. Based on the work displayed here, with further development vascular-focused PTT could be an effective strategy for the elimination of brain tumors.

## Conclusion

Overall, our results indicate that VEGF-NSs have further potential as a mediator of anti-angiogenic glioma therapy. *In vitro*, VEGF-NS bound VEGFR-2 expressing MS1 endothelial cells, which acted to mimic tumor vasculature, at levels sufficient for photothermal ablation. *In vivo*, more vascular-targeted NSs bound vessels associated with intracerebral tumors than nontargeted PEG-NSs and subsequent application of a near-infrared laser induced hyperthermia to disrupt the tumor vessels. Intravital microscopy images proved that sufficient heat was obtained to disrupt tumor vessels, as vessel density only decreased in mice that received VEGF-NSs following laser exposure. Furthermore, the area of the GFP signal (which indicates tumor size) remained fairly constant in VEGF-NS treated mice, but increased rapidly in mice treated with saline, indicating this vessel disruption slowed tumor growth. In turn, median survival time doubled in mice treated with VEGF-NS compared with mice treated with saline. Importantly, the normal brain was unaffected by treatment based on histological assessment. As this therapy is developed further it will be critical to continually evaluate the safety margin since brain tumor treatments are often plagued by long-term side effects.

To conclude, vascular-targeted NS-mediated PTT offers an intriguing alternative to conventional glioma treatments. PTT offers the advantage over chemotherapy and radiation therapy, in that it is quick and should prevent patients from enduring weeks or months of treatment. In addition, the procedure is simpler to perform and thus may pose less risk than surgery. In the future, vascular-targeted NS-mediated PTT could be an excellent treatment not only for gliomas, but also for a multitude of tumor types.

## Future perspective

Molecular targeting is anticipated to improve cancer nanomedicine by enhancing specificity, prolonging nanoparticle retention in the tumor and decreasing off-target effects. While the scientific community is making great strides towards this goal, there is still much work to be performed and knowledge to be gained before this potential will be fully realized. Several groups have tested targeting schemes *in vitro*, but *in vivo* validation is lacking. It is critical to evaluate these systems in animal models because in a complex biological setting it is more difficult to reach the target site. Here we provided an initial evaluation of vascular-targeted PTT

with VEGF-NSs, and the results suggest that this novel alternative to conventional glioma therapy is worthy of further investigation. Future work will include survival studies in larger animal models to confirm the results of this research, which demonstrated the proof-of-concept that tumor vessels can be disrupted with focused hyperthermia. It remains to be determined whether this disruption results in reduced oxygen and nutrient transport into the tumor that will ultimately lead to tumor necrosis and improved long-term survival; so answering these questions will be a major focus of our future studies.

### Acknowledgements

The authors thank X-N Li for training regarding intracerebral tumor models, N Ahmed for performing cell transfection, JH Slater for assistance with statistical analysis and image analysis, AJ Coughlin for help with SDS-PAGE and transmission electron microscopy, and N Chedid for support with *in vitro* studies.

### Financial & competing interests disclosure

This work was supported by the National Science Foundation EEC-0647452 (JL West), NIH R21 CA118788 (JL West), National Science Foundation Graduate Research Fellowship (ES Day), Hope Street Kids (PAT), NIH MSCIDA 3 U10 HD037242-08S1 (PA Thompson). JL West discloses a financial interest in Nanospectra Biosciences, Inc. The authors have no other relevant affiliations or financial involvement with any organization or entity with a financial interest in or financial conflict with the subject matter or materials discussed in the manuscript apart from those disclosed.

No writing assistance was utilized in the production of this manuscript.

### Ethical conduct of research

The authors state that they have obtained appropriate institutional review board approval or have followed the principles outlined in the Declaration of Helsinki for all human or animal experimental investigations. In addition, for investigations involving human subjects, informed consent has been obtained from the participants involved.

## Executive summary

### VEGF-conjugated nanoshells bind murine endothelial cells *in vitro* to facilitate photothermal therapy

- Nanoshells (NSs; silica core/gold shell nanoparticles) have been used successfully as a mediator of photothermal therapy (PTT) against a variety of tumor cell lines.
- Coating NSs with VEGF promoted their binding to endothelial cells expressing the appropriate receptor (VEGFR-2) *in vitro*.
- *In vitro* analysis confirmed the efficacy of vascular-targeted PTT and justified further investigation *in vivo*.

### VEGF-coated & PEG-coated NSs accumulate in intracerebral tumors

- This is the first report to assess the *in vivo* distribution of molecularly targeted NSs and to demonstrate the effect on intratumoral NS localization.
- Both PEG-coated and VEGF-coated NSs accumulated to a higher degree in intracerebral glioma tumors than in the normal brain.
- In this orthotopic glioma model, coating NSs with VEGF instead of with PEG nearly doubled the percentage of nanoparticles bound to tumor vessels.

### Intravital microscopy & histology indicate that NS-mediated PTT can disrupt tumor-associated vasculature

- Upon irradiation with a near-infrared laser, NSs bound to tumor vessels produced heat sufficient to induce vascular disruption and slow tumor growth.
- Minimal damage was observed in the normal brain following PTT.
- These data support continued studies of vascular-targeted PTT.

## References

Papers of special note have been highlighted as:

- of interest
- of considerable interest

- 1 Tuettenberg J, Friedel C, Vajkoczy P. Angiogenesis in malignant glioma – a target for antitumor therapy? *Crit. Rev. Oncol. Hematol.* 59(3), 181–193 (2006).
- 2 Day E, Thompson P, Zhang L *et al.* Nanoshell-mediated photothermal therapy improves survival in a murine glioma model. *J. Neurooncol.* 104(1), 55–63 (2011).
- Our previous work demonstrated that treatment of mice bearing subcutaneous glioma tumors with nanoshell-mediated photothermal therapy can induce tumor regression and prolong survival.
- 3 Day ES, Morton JG, West JL. Nanoparticles for thermal cancer therapy. *J. Biomech. Eng.* 131(7), 074001–074005 (2009).
- 4 Kennedy LC, Bickford LR, Lewinski NA *et al.* A new era for cancer treatment: gold-nanoparticle-mediated thermal therapies. *Small* 7(2), 169–183 (2011).
- 5 Erber R, Thurnher A, Katsen AD *et al.* Combined inhibition of VEGF and PDGF signaling enforces tumor vessel regression by interfering with pericyte-mediated endothelial cell survival mechanisms. *FASEB J.* 18(2), 338–340 (2004).
- 6 Keunen O, Johansson M, Oudin A *et al.* Anti-VEGF treatment reduces blood supply and increases tumor cell invasion in glioblastoma. *Proc. Natl Acad. Sci. USA* 108(9), 3749–3754 (2011).
- 7 Hirsch LR, Stafford RJ, Bankson JA *et al.* Nanoshell-mediated near-infrared thermal therapy of tumors under magnetic resonance guidance. *Proc. Natl Acad. Sci. USA* 100(23), 13549–13554 (2003).
- This seminal paper introduced nanoparticle-mediated photothermal therapy.
- 8 O’Neal DP, Hirsch LR, Halas NJ, Payne JD, West JL. Photo-thermal tumor ablation in mice using near infrared-absorbing nanoparticles. *Cancer Lett.* 209(2), 171–176 (2004).

- 9 Lu W, Xiong C, Zhang G *et al.* Targeted photothermal ablation of murine melanomas with melanocyte-stimulating hormone analog-conjugated hollow gold nanospheres. *Clin. Cancer Res.* 15(3), 876–886 (2009).
- 10 Dickerson EB, Dreaden EC, Huang XH *et al.* Gold nanorod assisted near-infrared plasmonic photothermal therapy (PPTT) of squamous cell carcinoma in mice. *Cancer Lett.* 269(1), 57–66 (2008).
- 11 Huang X, El-Sayed IH, Qian W, El-Sayed MA. Cancer cell imaging and photothermal therapy in the near-infrared region by using gold nanorods. *J. Am. Chem. Soc.* 128(6), 2115–2120 (2006).
- 12 Day ES, Bickford LR, Slater JH, Riggall NS, Drezek RA, West JL. Antibody-conjugated gold–gold sulfide nanoparticles as multifunctional agents for imaging and therapy of breast cancer. *Int. J. Nanomedicine* 5, 445–454 (2010).
- 13 Gobin AM, Warkins EM, Quevedo E, Colvin VL, West JL. Near-infrared-resonant gold/gold sulfide nanoparticles as a photothermal cancer therapeutic agent. *Small* 6(6), 745–752 (2010).
- 14 Au L, Zheng D, Zhou F, Li ZY, Li X, Xia Y. A quantitative study on the photothermal effect of immuno gold nanocages targeted to breast cancer cells. *ACS Nano* 2(8), 1645–1652 (2008).
- 15 Li Y, Lu W, Huang Q, Li C, Chen W. *In vitro* photothermal ablation of tumor cells with CuS nanoparticles. *Nanomedicine* 5(8), 1161–1171 (2010).
- 16 Zhou M, Zhang R, Huang M *et al.* A chelator-free multifunctional [<sup>64</sup>Cu]CuS nanoparticle platform for simultaneous micro-PET/CT imaging and photothermal ablation therapy. *J. Am. Chem. Soc.* 132(43), 15351–15358 (2010).
- 17 El-Sayed IH, Huang X, El-Sayed MA. Selective laser photo-thermal therapy of epithelial carcinoma using anti-EGFR antibody conjugated gold nanoparticles. *Cancer Lett.* 239(1), 129–135 (2006).
- 18 Cole JR, Mirin NA, Knight MW, Goodrich GP, Halas NJ. Photothermal efficiencies of nanoshells and nanorods for clinical therapeutic applications. *J. Phys. Chem. C* 113(28), 12090–12094 (2009).
- **Directly compares the optical properties of nanoshells, nanorods and gold–gold sulfide nanoparticles, which is critical to understanding their application in photothermal therapy.**
- 19 Chen J, Wang D, Xi J *et al.* Immuno gold nanocages with tailored optical properties for targeted photothermal destruction of cancer cells. *Nano Lett.* 7(5), 1318 (2007).
- 20 Lowery AR, Gobin AM, Day ES, Halas NJ, West JL. Immunonanoshells for targeted photothermal ablation of tumor cells. *Int. J. Nanomedicine* 1(2), 149–154 (2006).
- **One of the first articles to demonstrate that coating nanoshells with antibodies that bind surface receptors overexpressed on cancer cells can provide cell-specific photothermal therapy.**
- 21 Huang YF, Sefah K, Bamrungsap S, Chang HT, Tan W. Selective photothermal therapy for mixed cancer cells using aptamer-conjugated nanorods. *Langmuir* 24(20), 11860–11865 (2008).
- 22 Matsumura Y, Maeda H. A new concept for macromolecular therapeutics in cancer chemotherapy: mechanism of tumorotropic accumulation of proteins and the antitumor agent smancs. *Cancer Res.* 46(12 Part 1), 6387–6392 (1986).
- 23 Chamberlain MC. Antiangiogenesis: biology and utility in the treatment of gliomas. *Expert Rev. Neurother.* 8(10), 1419–1423 (2008).
- 24 Choudhury SR, Karmakar S, Banik NL, Ray SK. Role of Angiogenesis in the Pathogenesis of Glioblastoma and Antiangiogenic Therapies for Controlling Glioblastoma. In: *Glioblastoma: Molecular Mechanisms of Pathogenesis and Current Therapeutic Strategies*. Ray SK (Ed.). Springer, Berlin, Germany, 217–241 (2010).
- 25 Murphy EA, Majeti BK, Barnes LA *et al.* Nanoparticle-mediated drug delivery to tumor vasculature suppresses metastasis. *Proc. Natl Acad. Sci. USA* 105(27), 9343–9348 (2008).
- 26 Li Z, Huang P, Zhang X *et al.* RGD-conjugated dendrimer-modified gold nanorods for *in vivo* tumor targeting and photothermal therapy. *Mol. Pharm.* 7(1), 94–104 (2009).
- 27 Reardon DA, Wen PY, Desjardins A, Batchelor TT, Vredenburgh JJ. Glioblastoma multiforme: an emerging paradigm of anti-VEGF therapy. *Expert Opin. Biol. Ther.* 8(4), 541–553 (2008).
- **Highlights the development of anti-VEGF therapies for malignant glioma, discussing both the successes and the challenges to be overcome.**
- 28 Miletic H, Niclou SP, Johansson M, Bjerkvig R. Anti-VEGF therapies for malignant glioma: treatment effects and escape mechanisms. *Expert Opin. Ther. Targets* 13(4), 455–468 (2009).
- 29 Plate KH, Breier G, Weich HA, Mennel HD, Risau W. Vascular endothelial growth factor and glioma angiogenesis: coordinate induction of VEGF receptors, distribution of VEGF protein and possible *in vivo* regulatory mechanisms. *Int. J. Cancer* 59, 520–529 (1994).
- 30 Oldenburg SJ, Averitt RD, Westcott SL, Halas NJ. Nanoengineering of optical resonances. *Chem. Phys. Lett.* 288(2–4), 243–247 (1998).
- 31 Ahmed N, Ratnayake M, Savoldo B *et al.* Regression of experimental medulloblastoma following transfer of HER2-specific T cells. *Cancer Res.* 67(12), 5957–5964 (2007).
- 32 Gaber MW, Yuan H, Killmar JT, Naimark MD, Kiani MF, Merchant TE. An intravital microscopy study of radiation-induced changes in permeability and leukocyte-endothelial cell interactions in the microvessels of the rat pia mater and cremaster muscle. *Brain Res. Protoc.* 13, 1–10 (2004).
- 33 De Jong WH, Hagens WI, Krystek P, Burger MC, Sips A, Geertsma RE. Particle size-dependent organ distribution of gold nanoparticles after intravenous administration. *Biomaterials* 29(12), 1912–1919 (2008).
- 34 Niidome T, Yamagata M, Okamoto Y *et al.* PEG-modified gold nanorods with a stealth character for *in vivo* applications. *J. Control. Release* 114(3), 343–347 (2006).
- 35 Zhu X, Wu S, Dahut WL, Parikh CR. Risks of proteinuria and hypertension with bevacizumab, an antibody against vascular endothelial growth factor: systematic review and meta-analysis. *Am. J. Kidney Dis.* 49(2), 186–193 (2007).
- 36 Folkman J. Tumor angiogenesis: therapeutic implications. *N. Engl. J. Med.* 285(21), 1182–1186 (1971).
- 37 Carpin L, Bickford L, Agollah G *et al.* Immunoconjugated gold nanoshell-mediated photothermal ablation of trastuzumab-resistant breast cancer cells. *Breast Cancer Res. Treat.* 125(1), 27–34 (2011).
- 38 Knizetova P, Ehrmann J, Hlobilkova A *et al.* Autocrine regulation of glioblastoma cell cycle progression, viability and radioresistance through VEGF-VEGFR2 (KDR) interplay. *Cell Cycle* 7(16), 2553–2561 (2008).
- **Established that the VEGF signaling pathway promotes both autocrine and paracrine promotion of glioma tumorigenesis, making it an interesting therapeutic target.**
- 39 Choi CHJ, Alabi CA, Webster P, Davis ME. Mechanism of active targeting in solid tumors with transferrin-containing gold nanoparticles. *Proc. Natl Acad. Sci. USA* 107(3), 1235–1240 (2010).

- 40 Huang X, Peng X, Wang Y *et al.* A reexamination of active and passive tumor targeting by using rod-shaped gold nanocrystals and covalently conjugated peptide ligands. *ACS Nano* 4(10), 5887–5896 (2010).
- 41 Reddy GR, Bhojani MS, Mcconville P *et al.* Vascular targeted nanoparticles for imaging and treatment of brain tumors. *Clin. Cancer Res.* 12(22), 6677–6686 (2006).
- 42 Schwartz JA, Shetty AM, Price RE *et al.* Feasibility study of particle-assisted laser ablation of brain tumors in orthotopic canine model. *Cancer Res.* 69(4), 1659–1667 (2009).
- The feasibility of using fiber-optic probes to deliver light to tumors embedded in the brain is proven in this work; this is important for future development of nanoparticle-mediated photothermal therapy of brain tumors.
- 43 Deangelis LM. Brain tumors. *N. Engl. J. Med.* 344(2), 114–123 (2001).